SLAC-PUB-14338

FIRST RESULTS OF THE LCLS LASER-HEATER SYSTEM*

P. Emma, R. F. Boyce, A. Brachmann, R. Carr, F.-J. Decker, Y. Ding, D. Dowell, S. Edstrom, J. Frisch, S. Gilevich, G. Hays, Ph. Hering, Z. Huang, R. Iverson, Y. Levashov, H. Loos, A. Miahnahri, H.-D. Nuhn, B. Poling, D. Ratner, S. Spampinati†, J. Turner, J. Welch, W. White, Z. Wolf, J. Wu
SLAC, Menlo Park, CA 94025, USA

Abstract

The very bright electron beam required for an x-ray free-electron laser (FEL), such as the LCLS, is susceptible to a microbunching instability in the magnetic bunch compressors, prior to the FEL undulator. The uncorrelated electron energy spread in the LCLS can be increased by an order of magnitude to provide strong Landau damping against the instability without degrading the FEL performance. To this end, a 'laser-heater' system has been installed in the LCLS injector, which modulates the energy of a 135-MeV electron bunch with an IR laser beam in a short undulator, enclosed within a four-dipole chicane. The last half of the chicane time-smears the energy modulation leaving an effective thermal energy spread increase. We present the first commissioning results of this system, its operational issues, its impact on the microbunching instability, and finally its effect on the FEL performance.

INTRODUCTION

The Linac Coherent Light Source (LCLS) is an x-ray Free-Electron Laser (FEL) project that has just achieved its first lasing at 1.5 Å radiation wavelength [1]. The very bright electron beam required to drive this FEL is susceptible to a microbunching instability in the magnetic bunch compressors that may increase the slice energy spread beyond the FEL tolerance [2]. To control the slice energy spread and to suppress the microbunching instability, a laser heater (LH) system [2] is installed in the LCLS injector area at 135 MeV, right before the RF deflector that is used for the time-resolved electron diagnostics (see Fig 1). This unique component is used to add a small level of intrinsic energy spread to the electron beam in order to Landau damp the microbunching instability before it potentially breaks up the high brightness electron beam. The system was fully installed and tested in the fall of 2008, and effects of heating on the electron beam and the x-ray FEL were studied during the 2009 commissioning period.

The laser heater system is composed of a 4-dipole chicane; a 9-period, planar, permanent-magnet, adjustable-gap undulator at the center of the chicane; one OTR screen on each side of the undulator for electron/laser spatial alignment; and an IR laser (up to 15-MW power) which co-propagates with the electron beam inside the undulator generating a 758-nm energy modulation along the bunch. The final two dipoles of the 4-dipole chicane time-smear this modulation leaving only a thermal-like intrinsic energy spread within the bunch. Table 1 lists the main parameters for this system.

* Work supported by the U.S. DOE contract DE-AC02-76SF00515.
† Visiting from Sincrotrone Trieste, Trieste, Italy

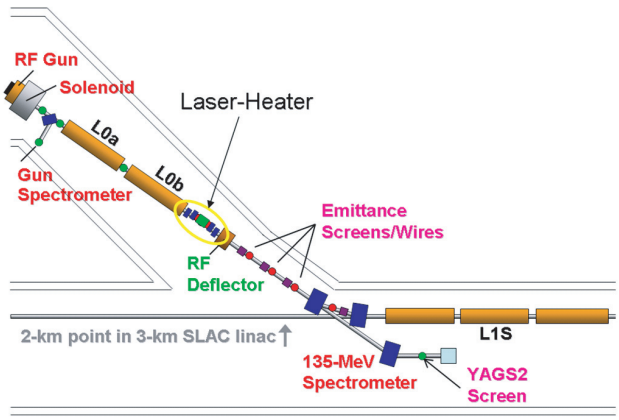

Figure 1: The LCLS injector layout showing laser heater, transverse RF deflector, OTR/YAG screens, wire scanners, and spectrometers.

Table 1: LCLS laser heater (LH) parameters (at 135 MeV).

Parameter	sym.	value	unit
LH-undulator pole full gap	g_u	34.5	mm
LH-undulator parameter	K	1.38	-
LH-undulator period	λ_u	5.4	cm
No. of full LH-undulator periods	N_u	9	-
IR laser wavelength	λ_L	758	nm
IR laser energy (nom 10 μJ)	E_L	< 230	μJ
IR laser pulse duration (FWHM)	T_L	15	ps
Hor. offset at center of chicane	Δx	35	mm
Bend angle of each dipole	$\|\theta\|$	7.5	deg
Electron & IR beam size in und.	$\sigma_{x,y}$	~ 180	μm
Laser Rayleigh length	Z_R	~ 50	cm

LASER HEATER SETUP

A portion of the infrared (IR) laser beam from the drive laser is guided by the IR beam transport optics from the laser room down to the accelerator tunnel (see Fig. 2). Laser diagnostics include two imaging cameras (VHC and CH1), power meter, photodiode for rough temporal overlapping, motorized controlled mirrors (MH2 and MH3) for position feedback control, an adjustable delay line, a waveplate, an attenuator, and a shutter for energy control.

Two 1-μm aluminum OTR screens are included with one on each side of the undulator in order to align the laser beam with respect to the electron beam transversely and to

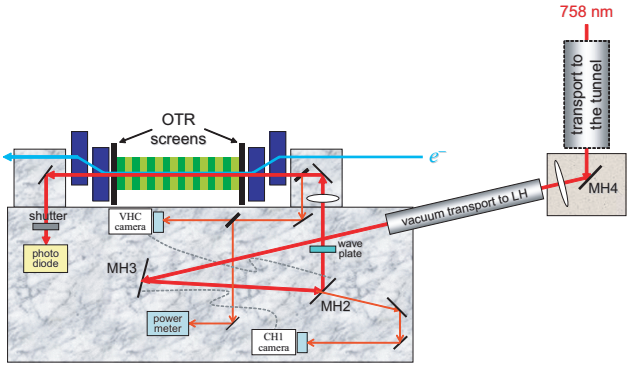

Figure 2: The layout of the laser heater system showing LH chicane, undulator, OTR screens, laser transport, motorized mirrors, cameras, waveplate, power meter, and photodiode.

measure the beam sizes. Since these thin OTR screens have shown damage with > 2 μJ of IR energy at 10 Hz beam repetition rate, they are protected from IR laser damage by logic which drops in a laser attenuator when either of the OTR screens are inserted. Figure 3 shows the individual images of the laser light and the optical radiation signal generated by the electron beam on the two OTR screens. The "electron" image on OTRH1 (the first OTR screen) shows both the OTR signal and synchrotron radiation from the second dipole (Fig 3(c)), while the "electron" image on OTRH2 (the second OTR screen) shows the OTR signal together with undulator radiation pattern (Fig 3(d)). The four lobes are the vertical polarization component of the fundamental undulator radiation. The motorized mirrors MH2 and MH3 adjust the offset positions of the laser centroid relative to the electron centroid until within ~ 100 μm tolerance level. The transverse alignment process has been automated using a Matlab-based GUI program.

A fast photodiode is used to sense the electron arrival time using the OTR light and to establish coincidence with the laser pulse within 10 ps. Finer timing adjustment is made manually by using the laser delay line in the laser room. When properly aligned in space and time, the laser-electron interaction will generate significant energy spread that are easily detected using the 135-MeV spectrometer shown in Fig. 1. The spectrometer is designed to have a very large dispersion ($\eta \approx 0.9$ m) and a small beta function ($\beta \approx 1$ m) on a YAG screen ("YAGS2") in order to have a few keV energy resolution.

MEASUREMENT OF HEATING EFFECTS

Figure 4 shows the measured beam profiles on YAGS2 for three different IR-laser pulse energy settings (0, 10 μJ, and 230 μJ). The transverse RF deflector (Fig. 1) is switched on here converting the vertical axis on YAGS2 to time (the bunch length coordinate), while the 135-MeV spectrometer bend converts the horizontal YAGS2 axis to energy, revealing longitudinal phase space and clearly demonstrating the time-sliced energy spread is increased with the IR laser. By zooming into a thin vertical slice of

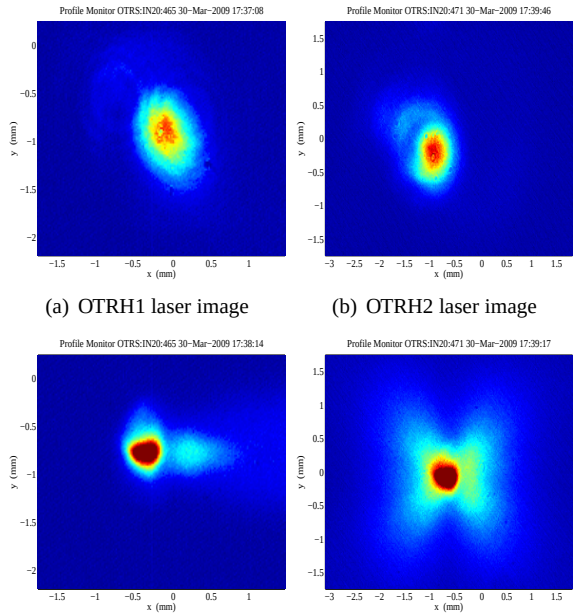

(a) OTRH1 laser image (b) OTRH2 laser image

(c) OTRH1 "electron" image (d) OTRH2 "electron" image

Figure 3: Beam images on LH OTR screens (OTRH1 and H2) before transverse alignment, see text for details.

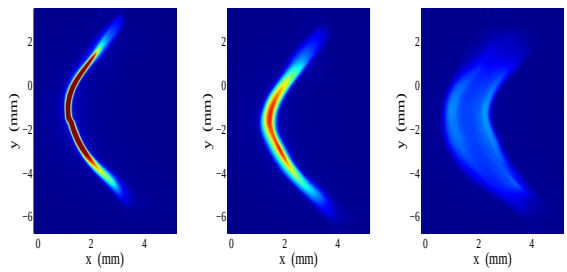

(a) no heating (b) nominal heating (c) maximum heating

Figure 4: Measured longitudinal phase space on "YAGS2" screen at 135 MeV with (a) laser heater off, (b) IR laser energy at 10 μJ, and (c) at 220 μJ.

YAGS2 profile, the slice energy distribution and the rms energy spread can be obtained as shown in Fig. 5 (at the maximum LH energy). The laser rms transverse size in the middle of the undulator can be imaged by the VHC camera (Fig 2) and is about 190 μm, while the electron beam size is about 150 μm based on the OTRH1 image. Thus, the laser spot size is somewhat larger than the electron spot size, resulting in the double-horn energy distribution (Fig. 5 (a)). The energy distribution is more Gaussian-like when the laser matches electron beam size in the undulator (Fig. 5 (b)) and is determined to be more effective in suppressing microbunching instability [2]. However, in order to overcome position jitter that may misalign the electron beam relative to the laser spot, we normally choose to have a slightly larger laser spot size than that of the electrons.

Figure 6 shows the measured central slice rms energy spread as a function of the LH energy. The calculated rms energy spread induced by the laser-electron interaction based on Eq. (8) of Ref. [2] is also shown for comparison

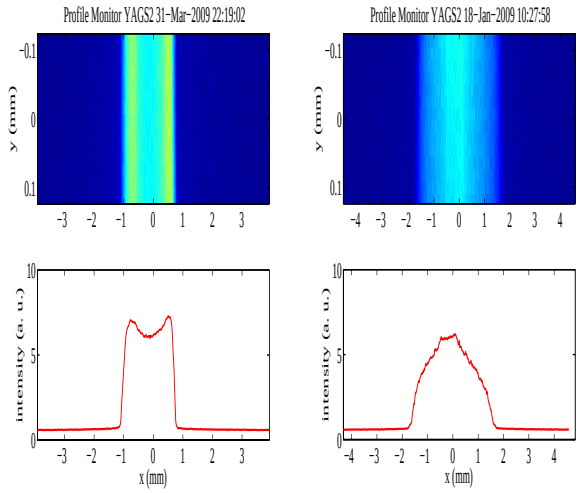

(a) Larger laser spot (b) Matched laser spot

Figure 5: Central slice images (upper plots) and horizontal profiles (lower plots) showing both the double horn (a) and more Gaussian-like (b) energy distribution.

(the rms is roughly a half of maximum modulation amplitude). When the laser heater shutter is closed, the measured slice energy spread is about 8 keV, limited by the horizontal beam size and YAG screen resolution. The intrinsic slice energy spread from simulations is around 2 to 3 keV. Nevertheless, for a very small amount of LH energy (< 5 μJ), we observe a sudden increase of heating effect on YAGS2 (the bump region in Fig. 6 at low heater energy). Because the nonzero R_{52} of the last half LH chicane, the 758-nm energy modulation is temporally smeared after the electron beam exiting the chicane. However, the coherent modulation may be restored at a particular section in the spectrometer dipole due to its opposite R_{52}. With a right amount of energy modulation and an overall R_{56} from the undulator to the spectrometer, the laser-induced energy modulation may then be converted to a large density modulation that can induce more energy spread through coherent radiation effects in the spectrometer dipole. The laser heater energy is normally set at ~ 10 μJ, corresponding to 25 keV rms energy spread measured on YAGS2 (slightly above the bump region). After a total compression ratio of $3000/37 \approx 80$, the slice energy spread becomes ~ 2 MeV or 1.5×10^{-4} at 13.64 GeV.

SUPPRESSION OF MICROBUNCHING INSTABILITY FOR THE LCLS FEL

Coherent optical radiation attributed to beam microbunching has been discovered during the LCLS commissioning [3, 4] that compromises the quantitative use of the many OTR screens downstream of the first bunch compressor. The laser heater suppresses these coherent signals by orders of magnitude in many cases but does not appear to completely remove a very small level of COTR after compression. Figure 7 shows the intensity of OTR22 (an OTR screen right after the second bunch compressor) vs

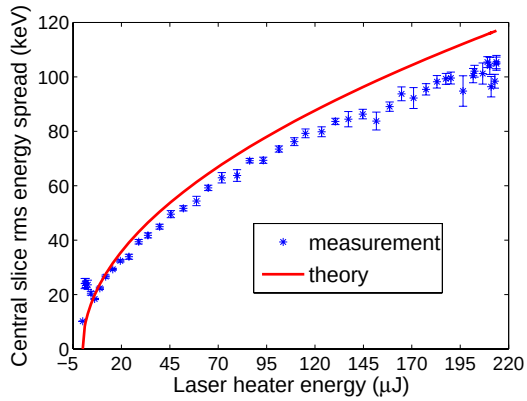

Figure 6: Central slice rms energy spread vs LH energy.

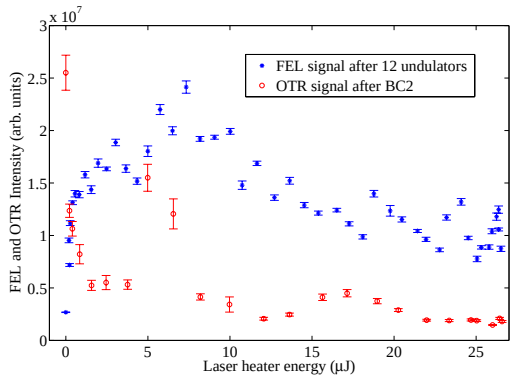

Figure 7: FEL and OTR intensities vs LH energy.

the laser heater energy from 0 to $\sim$ 27 μJ. We see that the COTR intensity drops sharply from its maximum (with LH off) and then starts to decay in an oscillatory behavior with the increasing LH energy. This non-exponential optical intensity decay may be explained by the non-Gaussian energy profiles created by the laser heating (see Fig. 5 and also Ref. [2]).

First lasing and saturation at the FEL wavelength of 1.5 Å has been achieved recently at the LCLS [1]. The FEL intensity measured on a downstream YAG screen vs. LH is illustrated in Fig. 7. Here 12 undulators are used to produce the x-rays where its intensity is still in the exponential growth regime and can be sensitive to microbunching instability. Figure 7 shows that the FEL power maximizes at about 7 μJ and drops by an order of magnitude without heating. This suggests that the laser heater adequately controls the slice energy spread for the LCLS FEL. Even when the FEL reaches saturation with 21 undulators, the FEL power still drops by at least a factor of 2 with LH off as compared to when the LH is set to ~ 7 μJ.

REFERENCES

[1] P. Emma *et al.*, these PAC2009 proceedings.

[2] Z. Huang *et al.*, Phys. Rev. ST-AB **7**, 074401 (2004).

[3] R. Akre *et. al.*, Phys. Rev. ST-AB **11**, 030703 (2008).

[4] H. Loos *et. al.*, FEL2008 Proc., Gyeongju, Korea, 2008.